LAWRENCE
LIVERMORE
NATIONAL
LABORATORY

LLNL-JRNL-416544

THE DIELECTRIC WALL ACCELERATOR

G. J. Caporaso, Y.-J. Chen, S. E. Sampayan

September 3, 2009

Reviews of Accelerator Science and Technology

Disclaimer

THE DIELECTRIC WALL ACCELERATOR*†

GEORGE J. CAPORASO
Lawrence Livermore National Laboratory, P.O. Box 808
Livermore, California 94551/, USA

YU-JIUAN CHEN
Lawrence Livermore National Laboratory, P.O. Box 808
Livermore, California 94551/, USA

STEPHEN E. SAMPAYAN
Lawrence Livermore National Laboratory, P.O. Box 808
Livermore, California 94551/, USA

The Dielectric Wall Accelerator (DWA), a class of induction accelerators, employs a novel insulating beam tube to impress a longitudinal electric field on a bunch of charged particles. The surface flashover characteristics of this tube may permit the attainment of accelerating gradients on the order of 100 MV/m for accelerating pulses on the order of a nanosecond in duration. A virtual traveling wave of excitation along the tube is produced at any desired speed by controlling the timing of pulse generating modules that supply a tangential electric field to the tube wall. Because of the ability to control the speed of this virtual wave, the accelerator is capable of handling any charge to mass ratio particle; hence it can be used for electrons, protons and any ion. The accelerator architectures, key technologies and development challenges will be described.

1. Introduction

1.1. *A New Type of Induction Accelerator*

Most particle accelerators employ metallic structures to produce the electric fields necessary for energy gain. These include cyclotrons, synchrotrons, RF linear accelerators and induction accelerators. These structures could be resonant cavities, accelerating cells and traveling or standing wave structures. Advanced techniques under active development use plasmas as the accelerating medium in which a large "wakefield" is excited by the passage of an intense laser pulse or charged particle bunch and accelerates a subsequent, less intense, "witness bunch". A version of this technique employs a dielectrically lined conducting tube and is known as a dielectric wall wakefield accelerator (not to be confused with the dielectric wall accelerator, the subject of this paper).

This article will describe accelerator concepts in which the beam tube is largely an insulator (the dielectric wall) that is energized by a pulsed power system. In order to prevent the accelerating voltages from appearing on the outside of the structure the accelerator is of necessity an induction accelerator [1]. While this type of accelerator is most suited for applications involving large beam currents, versions of it may be able to reach very high gradients that would make it suitable for low current applications like hadron therapy for cancer [2]. Although some of these ideas are not new, emerging technologies will permit their realization in the near term. And new ideas have been generated to capitalize on these emerging technologies.

1.2. *Induction Accelerator*

The DWA grew out of attempts to increase the gradient of induction accelerators, which were used primarily to handle large beam currents. Induction accelerators are comprised of electrically independent modules whose exterior surfaces are at ground potential. The

* This work was performed under the auspices of the U.S. Department of Energy by Lawrence Livermore National Laboratory under contract DE-AC52-07NA27344.

† Patents pending.

acceleration is produced non-resonantly and individual pulses may persist for up to microseconds. This is accomplished by employing inductive isolation provided by ferro- or ferri-magnetic cores inside the modules [3].

Figure 1 is a schematic of a typical induction module that is the basic building block of the accelerator. A voltage pulse enters the cell from a number of coaxial cables spaced azimuthally around the structure. There is a direct path for the voltage pulse down to the accelerating gap. However, there is also a DC short circuit from the center conductor of the cable around the inner surface of the cell back out to the shield of the cable. If the region encircled by this path contains magnetically permeable material substantial impedance to the flow of current around this path will exist as long as the material is not magnetically saturated.

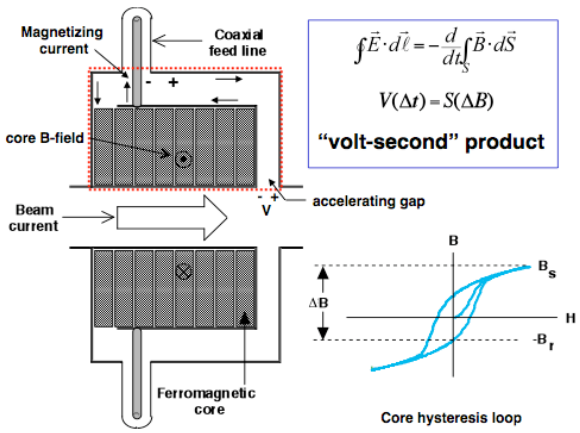

Figure 1. A typical induction cell. The integration contour (dotted line) can be used to apply Faraday's law. All contributions to the loop integral of the tangential electric field vanish except along the gap since all surfaces are conductors and the field reverses polarity in the cable. The core material has a B-H loop and is usually "reset" to a remnant value of magnetization in a direction opposite to that which the accelerating pulse would drive it in to increase the available flux swing (ΔB). Integrating Faraday's law with respect to time yields the "volt-second" product that is the time integral of the voltage, which can be sustained across the gap. This product is equal to the cross section area of the core multiplied by the flux swing.

While achievable electric field stresses across the (vacuum) accelerating gap may be in the range of 10 – 20 MV/m the overall, average gradient of machines made from these cells is usually less than 1 MV/m because of the relatively large amount of space occupied by the core. Since it is the cross section area of the core that is important for the volt-second product it is tempting to use a core that is short axially and larger radially to make up the area. However, all core material has substantial energy loss that is proportional to the core volume. Using cores that are axially long and thin in the radial direction will minimize the energy loss. Induction accelerators are low impedance devices that are well matched to beam currents on the order of kiloAmperes.

1.3. *Coreless Induction Accelerator*

Scientists in the former Soviet Union developed a coreless induction accelerator concept in 1970 [4] that had a more favorable aspect ratio than the previously described magnetic core version. In the schematic shown in Figure 2 the isolation is provided by the transit time of an electromagnetic wave from one line of the cell to the other.

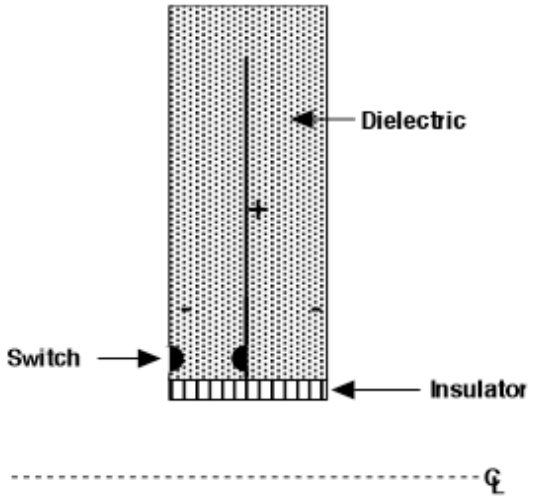

Figure 2. A coreless induction cell. The structure shown is azimuthally symmetric and is filled with a dielectric. The center conductor is charged with respect to the outer can. A closing switch is placed in close proximity to an insulator that separates the dielectric from the vacuum of the beam tube. There is no net voltage across the insulator until the switch closes. This voltage persists until the wave launched in the radial line by the switch closure has time to propagate up to the top and down the other side to the insulator.

The original cells use de-ionized water as the dielectric. The gradient achieved was approximately 1 MV/m. The radial lines had a relatively large radius to achieve a 25 ns pulsewidth. The performance of this line was limited by breakdown in the dielectric and vacuum insulator. Improvements in vacuum insulators, solid dielectrics and switches promise to increase the performance of such coreless cells by a large factor.

2. Concepts and Technologies to Increase the Gradient of Coreless Induction Accelerators

This section will discuss the innovations that have occurred in vacuum insulators, solid dielectrics and switches that will permit operation at elevated gradients.

2.1. *High Gradient Vacuum Insulators*

A key electrical weak point in the coreless induction cell of Figure 2 is the vacuum insulator. Vacuum surface flashover is not definitively understood. However, general trends can be discerned by examining published data. Failure of the insulator, i.e. surface flashover, occurs at a value of field stress that has an inverse dependence on the pulsewidth [5]. This key observation is the principal motivation for the accelerator mode to be discussed in section 3.

A novel insulator configuration, called a high gradient insulator (HGI), has the same inverse dependence of flashover field strength on pulsewidth but has superior performance [6]. The HGI is comprised of alternating layers of conductor and insulator with periods on the order of a mm or less.

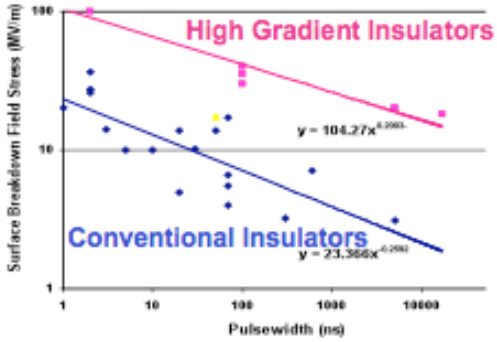

Figure 3. Dependence of vacuum surface flashover threshold vs. pulsewidth for conventional insulators (blue) and for HGI's (red). The general trend is an inverse dependence of flashover threshold on pulsewidth. The HGI's flashover threshold is several times that of monolithic insulators.

It is generally believed that field emission of electrons that repeatedly bombard the insulator surface and desorbs contaminant gas molecules is an essential precursor to surface flashover [7]. Studies of the trajectories of electrons near the surface of HGI's reveal a type of periodic focusing that tends to deflect these electrons away from the insulator surface [8] if the ratio of conductor to insulator thickness is in a certain range. This situation is depicted in Figure 4.

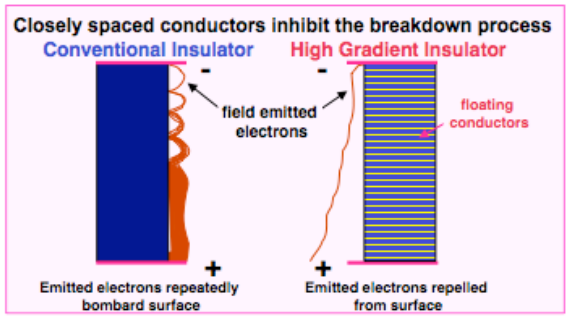

Figure 4. Flashover mechanism on a monolithic insulator is shown on the left hand side of the figure. A high gradient insulator is shown on the right hand side of the figure. Studies by Leopold and coworkers [7] showed that the periodic nature of the microstructure of the fields near the surface tends to deflect electrons away from the insulator surface. This observation may be important in explaining the improved performance of HGI's as compared to monolithic insulators.

2.2. *Solid Dielectrics*

It is very desirable to replace the liquid dielectric used in the original coreless induction cells with a solid dielectric. Development of a castable dielectric with high bulk breakdown strength and adjustable permittivity has been proceeding for some time [9]. This particular material is composed of nanoparticles of $BaSrTiO_2$ blended into various bases such as epoxy or silicone. The material is cast under vacuum and is virtually void free. Relative dielectric constants can vary between about 3 up to 45 by varying the density of nanoparticles. The material can be cast into large structures (over 1 m in length) and arbitrary shapes.

The bulk breakdown strength of the material is dependent upon the sample thickness and has demonstrated 400 MV/m for sub-millimeter thicknesses for low dielectric constant epoxy-based materials. A sample transmission line measuring 4 cm x 56 cm with embedded electrodes and an electrode separation of 0.8 mm is shown in Figure 5. This transmission line was charged repeatedly with 400 ns wide pulses at increasing voltages and finally failed at 141 kV or an average field stress of 170 MV/m.

Figure 5. A cast dielectric transmission line with embedded electrodes. The electrodes are separated by 0.8 mm and are 1 cm wide by 56 cm long. The dielectric is epoxy based with a relative dielectric constant of approximately 3. The sample failed at an average stress of 170 MV/m.

2.3. *Wide Band Gap Photoconductive Switches*

The coreless induction cell of Figure 2 has a closing switch whose function is to initiate the output voltage pulse. In order to achieve a high gradient in the cell the switch must be able to operate at a high electrical field stress.

There are other approaches employing opening switches that can be used for the DWA; these will be discussed in section 4.

Photoconductive switching of wide band gap materials such as SiC or GaN is compatible with very high voltage gradients [10]. The bulk breakdown strength of good quality SiC and GaN is in the range of 200 MV/m or higher.

The use of laser illumination having photon energies below the band gap permits one to take direct advantage of the high bulk breakdown strength of these materials. Light with energy below the band gap can propagate on the order of 1 – 2 cm in these materials permitting electrodes to be placed on opposite sides of a thin, large area wafer. By doping the material with appropriate concentrations of the right impurities, photoconductivity can be generated by laser illumination.

These switches can conduct over relatively wide areas (1 – 4 cm^2) and have a nearly ideal configuration for placement in pulse generating lines [11]. A switch schematic is depicted in Figure 6.

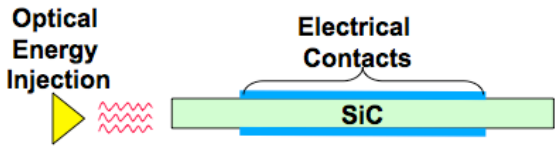

Figure 6. A typical wide band gap photoconductive switch is shown (in this case SiC). Placing electrodes on opposite sides of the wafer enables one to take direct advantage of the high bulk breakdown strength of these materials. Doping the wafer with the appropriate impurities leads to absorption of the laser light and the generation of photoconductivity.

An important feature of these devices is that the carriers recombine very rapidly (< 1ns) after removal of the laser illumination and recover even against full voltage. Thus, they act not only as closing switches but as opening switches as well. More precisely, they are light controlled resistors and can be operated in a linear regime at lower illumination levels [12].

A typical switch configured for testing in isolation (not in a pulse generating line) is shown in Figure 7.

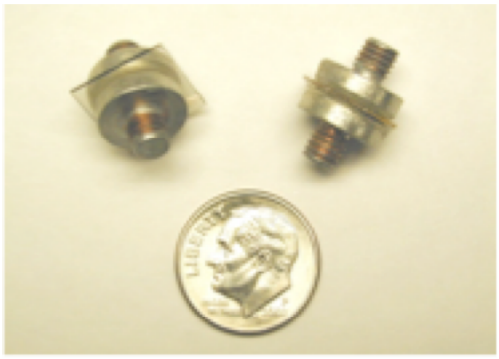

Figure 7. SiC wafers configured as switches for testing. The wafers measure 12 mm x 12 mm x 1 mm and are cut from A-plane 6H-SiC. Similar devices have been fabricated from 4H-SiC and GaN.

The ultimate design goal for a switch of the type and size shown in Figure 7 is about 100 kV corresponding to an average field stress in the material of 100 MV/m. Careful management of enhancements of the electric field at the electrode edges will be necessary to achieve this goal.

3. Sequential Pulse, Virtual Traveling Wave Accelerator

Because of the general inverse dependence of flashover threshold with pulsewidth shown in Figure 3, it would seem desirable to design pulse generating lines with the minimum possible output pulsewidth. However, in order to make the acceleration process efficient the particles should always be embedded in an accelerating field. In order that this be true the region of the dielectric wall exposed to high electric field must move along with the accelerating particles.

This can be accomplished if the coreless modules are relatively thin and are activated in sequence to produce a region of excitation along the wall that maintains synchronism with the charge bunch.

Maxwell's equations can then be used to impose a restriction on how short the pulsewidth may be in order to avoid dilution of the accelerating field on the axis of the tube [13].

3.1. *Pulsewidth Constraint*

We start by finding the axial electric field given its value along the tube wall. Inside the tube E_z satisfies the wave equation

$$\left(\nabla^2 - \frac{1}{c^2}\frac{\partial^2}{\partial t^2}\right)E_z = 0\,. \qquad (1)$$

Here E_z is the axial component of electric field. We seek a solution that is a function only of the "retarded time" variable $\tau = t-z/u$ where u is the speed of the excitation that is produced along the wall by sequential activation of the coreless induction modules. We consider the case where there is no azimuthal dependence. Then, inside the tube $E_z=E_z(r,\tau)$. Substituting this form into Eq. (1) and Fourier transforming in the variable τ to ω gives

$$\tilde{E}_z(r,\omega) = \tilde{E}_o(\omega)\frac{I_o\left(\frac{\omega r}{\gamma u}\right)}{I_o\left(\frac{\omega b}{\gamma u}\right)}. \qquad (2)$$

Here, b is the radius of the tube, $E_o(\tau)$ is the z-component of electric field along the wall of the tube and γ is the usual Lorentz factor, $(1-u^2/c^2)^{-1/2}$. The quantity I_o is the modified Bessel function of order zero.

Taking the inverse transform of Eq. (2) for a variety of trial functions for $E_o(\tau)$ such as a Gaussian, super-Gaussian and hyperbolic secant we obtain a nearly universal curve that expresses the ratio of E_z on axis to that on the wall of the tube as a function of the parameter $\theta=b/(\gamma u\tau_o)$. The parameter τ_o is the temporal full width at half maximum of the field at the wall at any given location. The spatial full width at half maximum of the field value at the wall is just $u\tau_o$.

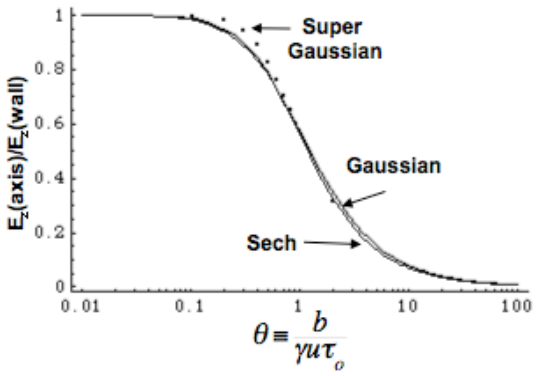

Figure 8. Nearly universal curve illustrating the dependence of the ratio of the on-axis value of the accelerating field to its value at the tube wall upon the parameter θ. For values of $\theta<0.3$ the on-axis field is comparable to its value at the wall.

From Figure 8 it can be seen that the on-axis field is comparable to that at the wall provided $\theta<0.3$. For highly relativistic particles this criterion can be satisfied for very short pulses. However for non-relativistic particles where γ is effectively unity, the criterion implies that the spatial full width at half maximum of the wall excitation > 3b.

4. Architectures for the DWA

There are several possible architectures for the DWA that involve different geometrical arrangements of pulse generating lines and which can employ closing or opening switches.

4.1. *Geometrical Choice*

There is a very wide variety of pulse generating lines employing closing switches that we generically refer to as "Blumleins". These lines are made up from 2 or more transmission lines [14].

Fundamental to the discussion of geometrical configurations is the characteristic impedance of a parallel plate transmission line, which depends on the dimensions of the line and the dielectric constant (we will assume that the relative permeability of the dielectric material is unity).

4.1.1 Classical Radial Line

For an azimuthally symmetrical structure the characteristic impedance is a function of the cylindrical radius and is given by

$$Z(r) = \sqrt{\frac{\mu_o}{\varepsilon}}\frac{d}{2\pi r} = \frac{60}{\sqrt{\varepsilon_r}}\frac{d}{r}\,Ohms. \qquad (3)$$

Here Z in the characteristic impedance, d is the axial separation between the plates, r is the cylindrical radius, ε is the actual dielectric constant and ε_r is the relative dielectric constant. Eq. (3) reveals that the characteristic impedance of the radial line varies with r. However, by tapering either d or ε or both with radius in the appropriate manner non-varying characteristic impedance can be achieved [13]. Eq. (3) implies that massive currents must flow when such a transmission line operates at high gradient. For example, if the gradient associated with a wave propagating in the line is 100 MV/m, and the relative dielectric constant is 3, a tube radius of 2 cm. will produce an associated current flow of 58 kA.

4.1.2 Strip Transmission Line Configuration

For a parallel plate transmission line the characteristic impedance is given by

$$Z = \sqrt{\frac{\mu_o}{\varepsilon}}\frac{d}{w} = \frac{120}{\sqrt{\varepsilon_r}}\frac{d}{w}\ Ohms. \qquad (4)$$

Here w is the transverse width of the plates and d is their separation.

An accelerator configured from strip "Blumleins" is shown in Figure 9. The end view is shown in Figure 10.

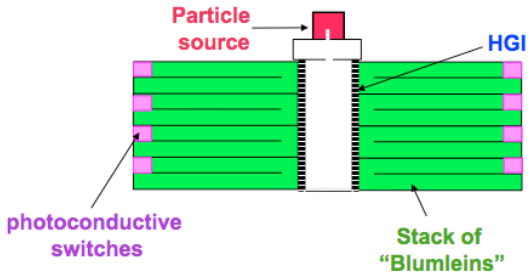

Figure 9. An example of a DWA using two stacks of "Blumleins" placed on opposite sides of the beam tube.

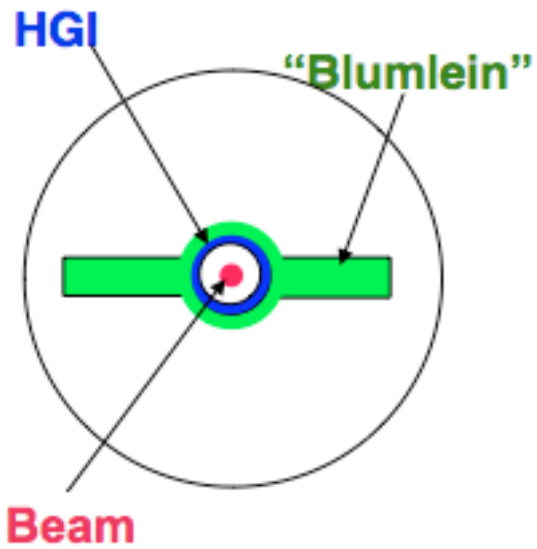

Figure 10. End view of the example shown in Figure 9 showing two stacks of strip "Blumleins" placed on opposites sides of the beam tube.

The strip "Blumlein" configuration can have considerably higher impedance than the radial line and requires fewer switches but suffers from parasitic coupling between different lines in the stack. The reason for this can be gleaned from examination of Figure 11.

A transmission line that is propagating a wave (launched by a switch closure for example) generates a magnetic field attendant to the current flow in the line (active line). Since the magnetic field is divergence free, the magnetic field lines must close.

In a radial line these field lines close azimuthally, but in a strip transmission line they close out of the plane of the line. In Figure 11 the line with current flow due to switch closure (the active line) produces magnetic field lines that close out of the plane of the line. If there is a nearby line (the passive line) that intercepts these field lines, a current will be induced in that line. The result of this current will be a reduction in the overall gradient of the stack and distortion of the temporal pulse produced by the lines [15].

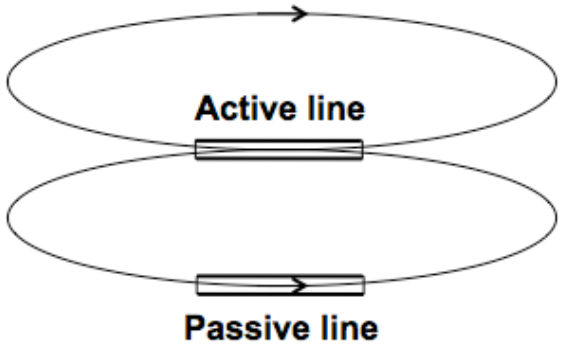

Figure 11. End view of two planar transmission lines. The active line is carrying a current produced by a switch closure or injection of a signal. The magnetic field lines produced by the current flow close out of the plane of the line and intercept nearby lines (the passive line). The intercepted magnetic field induces a current in the passive line. The net effect on a stack of pulse generating lines is a reduction in the output gradient and pulse distortion.

The effect of the parasitic coupling can be minimized by increasing the aspect ratio of the lines (i.e., by lowering their impedance). This problem motivated the invention of the architecture to be discussed in section 4.3.

4.2. *Pulse Generation Choices*

The coreless induction cell that we have been considering up to this point has employed closing switches. Schemes exist that employ opening switches [16].

One notable (the SLIM concept) example uses drift step recovery diodes as opening switches, which are

embedded in transmission lines [16]. These diodes conduct current and can then be controlled to open, generating a large voltage pulse that can be applied across an HGI. An example is shown in Figure 12.

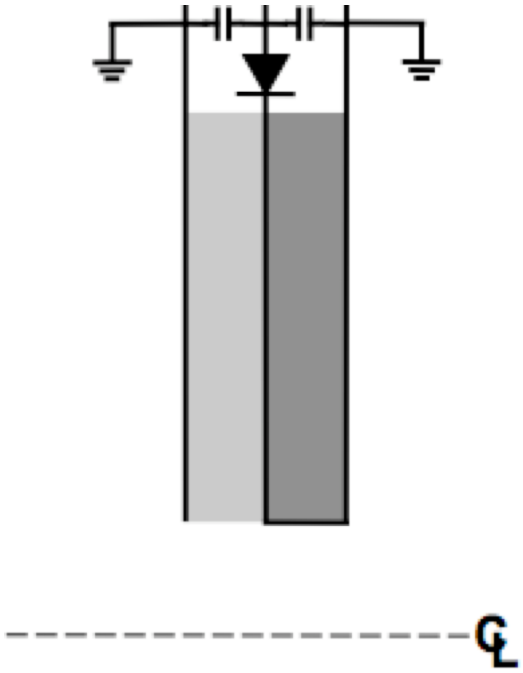

Figure 12. Illustration of an opening switch architecture using drift step recovery diodes (SLIM). When current flow in the diode is interrupted, a large, pulsed voltage appears across it that sends a wave down both transmission lines. The dark line on the right hand side is terminated in a short circuit while the lighter line on the left hand side is open and exposed to the beam tube. The line on the right side provides transit time isolation for the voltage pulse that appears across the bottom of the line on the left hand side.

The line shown in Figure 12 can be composed of separated strip transmission lines or it can be made into a radial line [17].

4.3. *Moving Virtual Gap Induction Concentrator*

A possible solution to the problem of parasitic coupling and the relatively low impedance of stacked "Blumlein" configuration is to use a structure that is placed entirely within conventional induction cells [15].

Consider the structure shown in Figure 13. It is an inductive voltage adder, a configuration that has been used for decades to sum up the voltages of a number of individual induction cells and impress it across a load. In Figure 13, the voltage of 9 cells appears across a single vacuum gap in an electron injector. The voltage of the entire structure is concentrated into the relatively small gap.

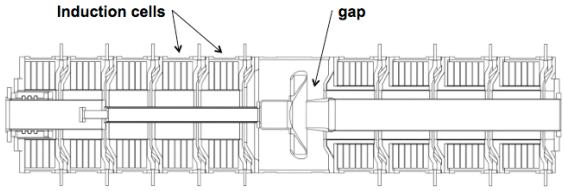

Figure 13. A diagram of an inductive voltage adder, in this case, an electron injector, is shown. The voltage of nine induction cells is summed together and appears across a relatively narrow vacuum gap. Thus, the voltage of the entire structure has been concentrated into a small region resulting in an electric field that is at least an order of magnitude greater than the average gradient of the structure.

Suppose we could arrange for the gap in Figure 13 to move in synchronism with an accelerating charge bunch. If that could be arranged, the particles would experience a continuous acceleration.

We could imagine replacing the interior of the inductive voltage adder with a stalk composed of a material whose conductivity could be varied on command. To create a virtual gap, the conductivity in the gap region would be relatively low while everywhere else it could be arranged to be very high so as to approximate a conducting tube with a vacuum gap.

This variable conductive material could be placed on the outer diameter of an HGI beam tube. If we could modulate the conductivity locally and rapidly enough, we could create a moving, virtual gap that would concentrate the voltage of the induction cells in a localized region. Photoconductive switches, in a variety of possible configurations, could be placed around the tube to provide this capability.

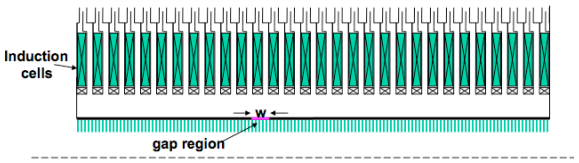

Figure 14. Inductive voltage adder schematic with a variable conductivity tube is illustrated. The virtual gap is of width w in the figure. The stalk is electrically connected to the induction cells at either end of the structure so that the electromagnetic fields are completely enclosed and no voltage appears on the exterior of the assembly.

It is clear that this concentration can occur for DC voltages. In order to assess to what degree this mechanism is viable for fast pulses, it is convenient to use a transmission line model of the induction system and conductive stalk.

In the simplest possible model we represent the induction cells by ideal voltage sources and use series inductance per unit length to describe the vacuum inductance of the stalk inside the cells. We also add a shunt capacitance per unit length to describe the distributed capacitance between the stalk and the inner surface of the cells. Finally, we represent the conductivity of the tube by a variable series resistance, R, per unit length.

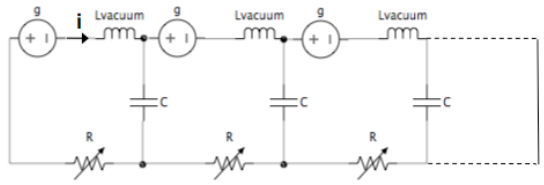

Figure 15. Simple circuit model of the inductive voltage adder with a variable conductivity stalk is illustrated. The variable resistors represent the locally variable conductivity of the stalk. The induction cells are represented by ideal voltage sources of g volts per unit length. The coaxial distributed inductance and capacitance are represented by the series L and shunt C respectively.

Using the circuit in Figure 15, we may write down equations for the voltage and current as

$$\frac{\partial V}{\partial x} = g(t,x) - L\frac{\partial i}{\partial t} - R(t,x)i \tag{5}$$

$$\frac{\partial i}{\partial x} = -C\frac{\partial V}{\partial t}. \tag{6}$$

Here, x is the distance along the beam axis, g represents the voltage produced by the induction cells, L and C represent the distributed stalk inductance and capacitance respectively, and R represents the variable conductivity tube.

The electric field parallel to the tube E_a, which is just the accelerating field, is given simply by

$$E_a = -R(t,x)i. \tag{7}$$

It will prove convenient to define dimensionless dependent and independent variables

$$\eta = \frac{R_o t}{L},\ \xi = \frac{x}{w},\ \psi = \frac{R_o i}{g_o},\ \Omega = \frac{V}{g_o w} \tag{8}$$

which are respectively, dimensionless time, axial distance, current and line voltage. Here, g_o is the maximum source gradient, R_o is the minimum resistance per unit length of the tube, and w is the axial extent of the virtual gap. The resistance of the tube and the source voltage per unit length (source function) are given by

$$R(\eta,\xi) = R_o f(\eta,\xi),\ g(\eta,\xi) = g_o \hat{g}(\eta,\xi). \tag{9}$$

We are seeking a localized pulse of electric field that occupies a relatively small fraction of the induction system. As an approximation, we seek a traveling wave solution of invariant form for Eqs. (5) – (9). Numerical solutions for a finite length system with the proper boundary conditions verify the validity of this approach. We specify a traveling wave of resistance along the tube as

$$f(\eta,\xi) = f\left(\frac{Lu}{R_o w}\eta - \xi\right) = f(\sigma) \tag{10}$$

where u is the speed of the virtual gap and σ is the independent variable. With this specification the system of equations (5) – (10) can be reduced to

$$\frac{\left(1 - LCu^2\right)}{wR_oCu}\frac{\partial \psi}{\partial \sigma} - f(\sigma)\psi = 1 \tag{11}$$

with

$$E_a = -g_o f(\sigma)\psi(\sigma) \tag{12}$$

where we have set the source function to 1.

Examination of Eq. (11) reveals that there are two distinct regimes: "subluminal" with $1\text{-}LCu^2 > 0$, and "superluminal" where $1\text{-}LCu^2 < 0$. This terminology arises from the fact that the speed of an electromagnetic wave along the coaxial system formed by the stalk and the inner surface of the induction cells is given by $1/(LC)^{1/2}$. The subluminal (superluminal) regime occurs when the speed of the virtual wave is less than (greater than) the wave propagation speed.

By demanding that the electric field be constant over the interval $0 < \sigma < 1$ (the gap) we can use Eq. (11) to solve for the current. Eq. (12) can then be used to determine the functional form for f(σ). Analysis of this case reveals that in the strongly subluminal regime the maximum gain, or field concentration is

$$\frac{E_a}{g_o} = 1 + \frac{1}{wR_oCu} \tag{13}$$

while for the strongly superluminal regime the maximum gain is given by

$$\frac{E_a}{g_o} = 1 + \frac{Lu}{R_o w}. \qquad (14)$$

As a particle speed increases it can be seen from Eq. (13) that the gain decreases. At some point, a transition to the superluminal regime would be appropriate. In order to produce a large potential gain the stalk could be loaded with magnetically permeable cores to increase the series inductance per unit length as is depicted in Figure 16.

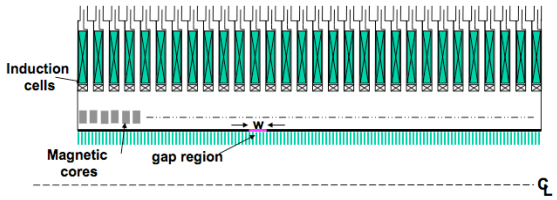

Figure 16. Magnetically permeable cores have been added around the conducting stalk to increase the series inductance per unit length. This can increase the potential gain in the superluminal regime.

Note that the circuit diagram corresponding to Figure 16 is identical to that of Figure 15 with an increased value of series inductance.

There is a dual to the circuit of Figure 15 in which the series resistance and inductance are interchanged. The series inductance can be provided by helix while the switches can be placed inside the induction cells. The switches are placed in series with a charged capacitor bank and the induction gaps to power the cells. This arrangement is shown in Figure 17.

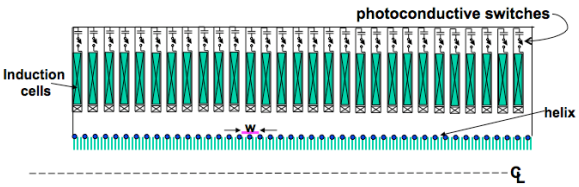

Figure 17. Dual configuration of the one in Figure 16 for the superluminal regime is shown. The series inductance per unit length of the system is now provided by a helical conductor around the dielectric beam tube. The switches are now inside the induction cells where they provide power to the cells by connecting a charged capacitor bank to the induction gaps.

For this configuration we must also consider the loss in the cores inside the cells, which appear in parallel with the switches. It is possible to add a core resistance in parallel with the switch resistance and obtain another traveling wave solution.

A solution for this case is shown in Figure 18 corresponding to an exponential increase in switch resistance after the removal of laser light. This is an appropriate approximation to describe the resistance change of a switch as the carriers recombine.

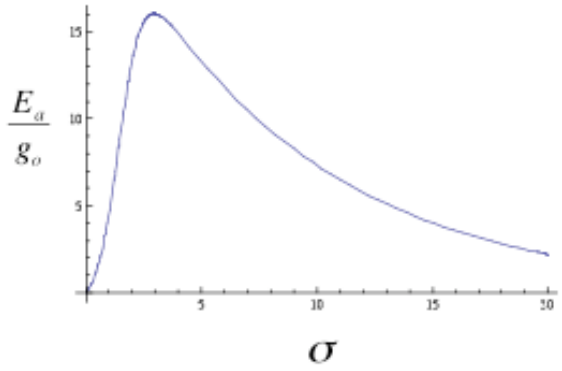

Figure 18. Traveling wave solution for the configuration of Figure 17 is shown. The gain is plotted as a function of the traveling wave similarity variable for the case of exponential increase of switch resistance after removal of laser light from the photoconductive switches.

The results shown in Figure 18 may be compared against a numerical solution of a finite length problem with the same parameters shown in Figure 19 for the case of constant u.

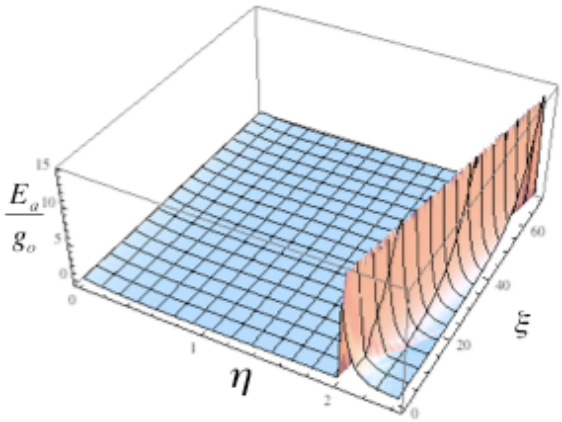

Figure 19. The full numerical solution for the architecture shown in Figure 17 is plotted as a function of dimensionless time and distance. The model includes a resistance in parallel with the switches to account for the loss of the magnetic cores in the induction cells. The amplitude and shape of the accelerating field agree very well with the traveling wave solution shown in Figure 18.

Note that the gain in this scheme is dependent upon rapid increases in the resistivity of the switches upon interruption of laser illumination. In this respect, this scheme is similar to those employing opening switches.

5. Challenges and Prospects

Some features of the various approaches that have been discussed are summarized in Table 1. Both the stripline and radial line options refer to either the use of "Blumleins" with closing switches or geometries similar to that of Figure 12 with opening switches. It appears that with either of the first two options external focusing can only be used if the structure is interrupted to insert lenses between the cells.

Table 1. Summary of accelerator architecture features for the options discussed. Notes in the table: *Unless terminated with a matched resistive or beam load. **In addition to switch, dielectric material and HGI limitations of the other architectures. ***Unless the cells are separated to allow focusing between them.

Architecture	Stripline	Radial Line	Induction Concentrator
Parasitic coupling	Yes	No	No
Impedance	Low	Very low	Low to moderate
Switch count	High	Very high	Moderate to high
Input power	High	Very high	Moderate to high
Ringing output	Yes*	Yes*	No
Gradient	High	Highest	Core may limit**
Waveform control	Limited	Moderate	Moderate
External focusing	No***	No***	Yes

Electrical strengths of newly developed dielectric and switch materials are consistent with gradients of 100 MV/m and small sample tests of HGI's have shown vacuum surface flashover thresholds of 100 MV/m for 3 ns pulses. Accelerator architectures have been devised that should be able to capitalize on these technological improvements and lead to the advent of short pulse, high gradient accelerators.

Acknowledgments

It is a pleasure to acknowledge the support of Drs. Cherry Murray and Bill Goldstein, as well as the support from members of the Beam Research Program at Lawrence Livermore National Laboratory and our TomoTherapy, Inc. and CPAC coworkers. One of the authors (G.J.C.) is indebted to Dr. Anatoly Krasnykh of SLAC for providing him with information on his SLIM concept. Support for this work was provided by Lawrence Livermore National Laboratory, U.C. Davis Cancer Center, TomoTherapy, Inc. and CPAC.

References

1. C. Kapetankos and P. Sprangle, *Physics Today* Feb**.**, 58 (1985).
2. M. Goitein, A. Lomax and E. Pedroni, *Physics Today Sept.*, 45 (2002). G. Caporaso, et. al., *Physica Medica* **24**, pg. 98 (2008).
3. N. Christofilos, R. Hester, H. Lamb, D. Reagan, H. Sherwood and R. Wright, *Rev. Sci. Inst.* **35**, 886 (1964).
4. A. Pavlovski, et. al., *Sov. At. En.* **28**, pg. 549 (1970).
5. S. Sampayan et. al., *IEEE Trans. Diel. And Elec. Ins.* **7**(3), pg. 334 (2000).
6. J Harris, et. al., *Appl. Phys. Lett.* **93**, pg. 241502 (2008).
7. R. Anderson and J. Brainard, *J. Appl. Phys.* **51**(3), pg. 1414 (1980).
8. J. Leopold, et. al., *IEEE Trans. Diel. And Elec. Ins.* **12**(3), pg. 530 (2005).
9. Sampayan and Sanders TPL reference
10. Sullivan or Nunnally on switch concept.
11. J. Sullivan and J. Stanley, "6H-SiC Photoconductive Switches Triggered Below Bandgap Wavelengths", in Proc. 27th Int. Modulator Symposium and 2006 High Voltage Workshop, Wash., D.C., 2006.
12. Sampayan or Sullivan on switch modulation
13. G. Caporaso, et. al., "High Gradient Induction Accelerator", in Proc. 2007 Particle Accelerator Conf. TUYC02.
14. M. Rhodes, "Ferrite-Free Stacked Blumlein Pulse Generator for Compact Induction Linacs", in *Proc. Pulsed Power Conf.* (2005).
15. G. Caporaso, et. al., "Status of the Dielectric Wall Accelerator", in Proc. 2009 Particle Accelerator Conf. TH3GAI02.
16. F. Arntz, A. Kardo-Sysoev and A. Krasnykh, "SLIM, Short-pulse Technology for High Gradient Induction Accelerators", SLAC-PUB-13477, 2008.
17. A. Krasnykh, "Evaluation of SLIM for Hadron Therapy", private communication, (2009).